

The Non-monotonicity of Moist Adiabatic Warming

OSAMU MIYAWAKI^a

^a *Department of Geosciences, Union College, Schenectady New York, USA*

ABSTRACT:

1. Introduction

The Clausius-Clapeyron relation implies the potential for a warmer atmosphere to hold more water vapor (Emanuel 1994). This principle is the basis for the positive water vapor feedback (Held and Soden 2000). It also underpins various scaling theories for climate responses to warming, including extreme precipitation, the Hadley cell edge, jet stream position, tropopause height, and convective available potential energy (CAPE; O’Gorman 2015; Shaw and Voigt 2016; Romps 2016).

In the tropics, convection couples the surface to the free troposphere. Because the timescale of radiative cooling is slower (order of days) compared to convection (order of hours), the tropical atmosphere is to first order in a state of quasi-equilibrium where the climatological free-tropospheric temperature follows a convectively neutral profile set by the surface temperature and humidity Arakawa and Schubert (1974). Although processes like convective entrainment influence the details of this coupling (Miyawaki et al. 2020; Keil et al. 2021), moist adiabatic adjustment is a useful first-order approximation (Held 1993). The top-heavy warming profile predicted by moist adiabatic adjustment (Fig. 1b) is a robust feature in climate models and observations, despite historical challenges in observational records (Vallis et al. 2015; Santer et al. 2005).

The top-heavy warming profile predicted by the moist adiabat is important because it increases dry static stability. Spatial variations in dry static stability influence the structure of tropical convergence zones because horizontal free-tropospheric gradients, while weak, exist (Neelin and Held 1987; Bao et al. 2022). This structure also defines the tropical lapse rate feedback, a key negative feedback for global climate sensitivity (Hansen et al. 1984). The lapse rate feedback partially cancels the water vapor feedback and scales in tandem because amplified warming in the upper troposphere is a consequence of increased surface water vapor and latent heat release (Held and Shell 2012). In a moist adiabatic atmosphere that is saturated at the surface, total latent heat release is $L_v(q_s^* - q_{\text{top}}^*)$ where L_v is the latent heat of vaporization, q_s^* is surface saturation

specific humidity, and q_{top}^* is the cloud top saturation specific humidity. $q_{\text{top}}^* \rightarrow 0$ as $T \rightarrow 0$ in a moist adiabatic atmosphere because the moist adiabat does not predict a stratosphere¹. Thus we expect total latent heat release in a moist adiabatic atmosphere to scale as q_s^* , which increases monotonically with surface temperature as expected from the Clausius-Clapeyron relation (Fig. 1a).

Given the monotonic increase in surface specific humidity with temperature, one might expect moist adiabatic warming to also increase monotonically with the initial surface temperature at all levels. However, moist adiabatic warming is a non-monotonic function of initial surface temperature (Fig. 1c, see Appendix A for details on calculating the moist adiabat). The non-monotonicity emerges in height coordinates (Fig. A1), with or without latent heat of fusion (see Appendix B and Fig. B1), and across different empirical formula for saturation vapor pressure (see Appendix C and Fig. C1). While previous work has acknowledged the existence of this non-monotonicity (Byrne and O’Gorman 2013; Levine and Boos 2016), an explanation does not yet exist in the literature.

This raises the question: what physical mechanism drives the non-monotonicity of moist adiabatic warming? Here we explain the origin of the non-monotonicity in moist adiabatic warming and its cascading effects on buoyancy and vertical velocity.

2. Theory of Non-Monotonic Warming

We start by defining the moist adiabatic temperature profile in pressure coordinates $T(p)$ in terms of the moist adiabatic lapse rate $\Gamma_m = dT/dp$:

$$T(p) = T_s + \int_{p_s}^p \Gamma_m dp' \quad (1)$$

where T_s is surface temperature. We assume the atmosphere is saturated from the surface. The difference be-

¹Romps (2016) shows how q_{top}^* varies with T_s assuming a fixed tropopause temperature = 200 K (see Hartmann and Larson 2002; Seeley et al. 2019, for evidence supporting this assumption). q_{top}^* exhibits super Clausius-Clapeyron scaling because of decreasing cloud top pressure with warming.

Corresponding author: Osamu Miyawaki, miyawako@union.edu

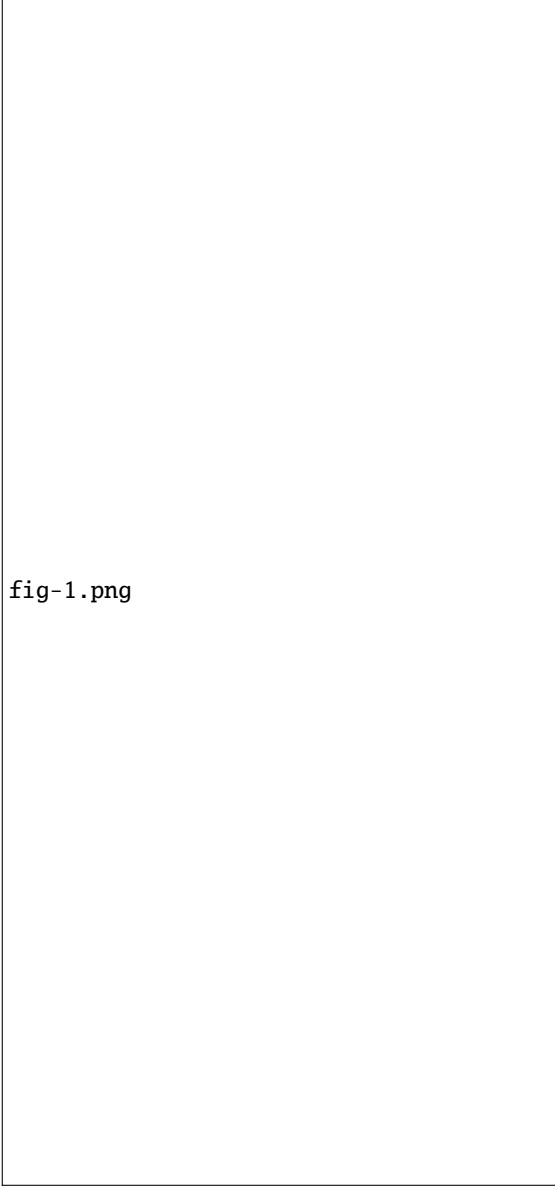


FIG. 1. (a) Surface saturation specific humidity increases monotonically with surface temperature. (b) Vertical profiles of moist adiabatic warming to a 4 K surface warming for $T_s = 280, 290, 300, 310,$ and 320 K. Warming decreases with initial surface temperature at lower levels while it increases with initial surface temperature at higher levels. (c) Moist adiabatic warming varies non-monotonically with initial surface temperature at all levels, e.g. at 500, 400, 300, and 200 hPa. Moist adiabatic warming peaks at warmer initial surface temperatures at higher levels.

tween a perturbed and baseline state (Δ) then follows as

$$\Delta T(p) = \Delta T_s + \int_{p_s}^p \Delta \Gamma_m dp' \quad (2)$$

For a small perturbation, $\Delta \Gamma_m$ can be approximated using a first-order Taylor expansion: $\Delta \Gamma_m \approx \frac{d\Gamma_m}{dT_s} \Delta T_s$. Substituting this into Eq. (2) gives

$$\Delta T(p) \approx \Delta T_s + \left(\int_{p_s}^p \frac{d\Gamma_m}{dT_s} dp' \right) \Delta T_s \quad (3)$$

The non-monotonicity in moist adiabatic warming is encoded into $d\Gamma_m/dT_s$, the sensitivity of the moist adiabatic lapse rate to surface temperature. Indeed, $d\Gamma_m/dT_s$ is non-monotonic with respect to temperature (dashed line shows the local minima of $d\Gamma_m/dT_s$ in Fig. 2a). Note that $d\Gamma_m/dT_s$ is mostly negative in the troposphere (Fig. 2b). This is consistent with amplified warming aloft because the integral in Eq. (2) is from high to low pressure, which introduces a negative sign.

Γ_m is a function of local temperature and pressure $\Gamma_m(T, p)$. To make progress in understanding $d\Gamma_m/dT_s$, we must rewrite $d\Gamma_m/dT_s$ in terms of derivatives with respect to the local state variables (T, p) . To do this we first use the chain rule:

$$\frac{d\Gamma_m}{dT_s} = \left(\frac{\partial \Gamma_m}{\partial T} \right)_p \cdot \frac{dT}{dT_s} + \left(\frac{\partial \Gamma_m}{\partial p} \right)_T \cdot \frac{dp}{dT_s} \quad (4)$$

The second term $\frac{dp}{dT_s} = 0$ because pressure, being the vertical coordinate, is independent of surface temperature. Recognizing that by definition $\Gamma_m = \frac{dT}{dp}$,

$$\frac{d}{dp} \left(\frac{dT}{dT_s} \right) = \left(\frac{\partial \Gamma_m}{\partial T} \right)_p \cdot \frac{dT}{dT_s} \quad (5)$$

This is an ordinary differential equation for $\frac{dT}{dT_s}$ as a function of pressure. The solution with the boundary condition $\frac{dT}{dT_s}(p_s) = 1$, is

$$\frac{dT}{dT_s} = \exp \left(\int_{p_s}^p \left(\frac{\partial \Gamma_m}{\partial T} \right)_p dp' \right) \quad (6)$$

Substituting Eq. (6) into Eq. (4) gives

$$\frac{d\Gamma_m}{dT_s} = \left(\frac{\partial \Gamma_m}{\partial T} \right)_p \cdot \exp \left(\int_{p_s}^p \left(\frac{\partial \Gamma_m}{\partial T} \right)_p dp' \right) \quad (7)$$

where $(\partial \Gamma_m / \partial T)_p$ is the moist adiabatic lapse rate sensitivity to local temperature T at pressure level p . The integral describes how a small surface temperature perturbation dT_s influences $\Gamma_m(T, p)$ through the sum of all Γ_m changes that occur below pressure level p .

The non-monotonicity can arise from either 1) $\partial \Gamma_m / \partial T$ being non-monotonic and the integral acting to amplify it or 2) $\partial \Gamma_m / \partial T$ being monotonic but sign changes in $\partial \Gamma_m / \partial T$ leads to the integral being non-monotonic. Numerical solutions show that $\partial \Gamma_m / \partial T$ is non-monotonic (dash-dot line

shows the local minima of $\partial\Gamma_m/\partial T$ in Fig. 2c). The integral term amplifies this non-monotonicity (Fig. 2d).

Why is $\partial\Gamma_m/\partial T$ non-monotonic? To understand this we solve for Γ_m from the first law of thermodynamics for adiabatic, non-precipitating, and reversible ascent of a saturated air parcel:

$$c_p dT - \alpha dp + L_v dq^* = 0 \quad (8)$$

where c_p is the specific heat capacity of air at constant pressure, α is specific volume, L_v is the latent heat of vaporization, and q^* is the saturation specific humidity. We assume 1) $c_p \approx c_{pd}$, neglecting the role of water of all phases on the specific heat capacity and 2) $\alpha \approx \alpha_d = R_d T/p$, neglecting the virtual effect of water vapor on density.

Next we use the chain rule to expand dq^* :

$$dq^* = \left(\frac{\partial q^*}{\partial T} \right)_p dT + \left(\frac{\partial q^*}{\partial p} \right)_T dp \quad (9)$$

Substituting Eq. (9) into Eq. (8) and rearranging gives

$$\left(c_{pd} + L_v \left(\frac{\partial q^*}{\partial T} \right)_p \right) dT = \left(\alpha_d - L_v \left(\frac{\partial q^*}{\partial p} \right)_T \right) dp \quad (10)$$

We can derive closed-form expressions for the q^* derivatives using the Clausius-Clapeyron relation and Dalton's Law. These q^* derivatives describe the role of phase equilibrium shifts in q^* with T and p on the effective heat capacity and specific volume of the air parcel, respectively:

$$c_L \equiv L_v \left(\frac{\partial q^*}{\partial T} \right)_p \approx \frac{L_v^2 q^*}{R_v T^2} \quad (11)$$

$$\alpha_L \equiv -L_v \left(\frac{\partial q^*}{\partial p} \right)_T \approx \frac{L_v q^*}{p} \quad (12)$$

where the approximation arises from assuming saturation vapor pressure $e^* \ll p$.

c_L can be thought of as a latent heat capacity, which represents the increase in thermal inertia as latent heating cancels part of the cooling from expansion. c_L acts to increase the heat capacity of the air parcel such that it has an effective heat capacity $c_{pd} + c_L$.

α_L can be thought of as a latent specific volume, which represents the enhanced expansion of air with ascent as lower pressure shifts the phase equilibrium of water toward the vapor phase. α_L acts to increase the volume of air such that it has an effective specific volume $\alpha_d + \alpha_L$.

Solving for the moist adiabatic lapse rate $\Gamma_m = dT/dp$:

$$\Gamma_m = \frac{dT}{dp} = \frac{\alpha_d + \alpha_L}{c_{pd} + c_L} \quad (13)$$

$$= \Gamma_d \cdot \frac{1 + \frac{\alpha_L}{\alpha_d}}{1 + \frac{c_L}{c_{pd}}} \quad (14)$$

where $\Gamma_d = \alpha_d/c_{pd}$ is the dry adiabatic lapse rate in pressure coordinates and the two non-dimensional terms represent the fractional increase in effective specific heat capacity and specific volume due to the pressure and temperature sensitivities of the phase equilibrium of water:

$$\tilde{c} = \frac{c_L}{c_{pd}} = \frac{L_v^2 q^*}{c_{pd} R_v T^2} \quad (15)$$

$$\tilde{\alpha} = \frac{\alpha_L}{\alpha_d} = \frac{L_v q^*}{R_d T} = \frac{R_v c_{pd} T}{R_d L_v} \tilde{c} = k \tilde{c} \quad (16)$$

Substituting Eq. (15) and Eq. (16) into Eq. (14) gives

$$\Gamma_m = \Gamma_d \cdot \frac{1 + k \tilde{c}}{1 + \tilde{c}} \quad (17)$$

For typical values in Earth's atmosphere ($R_v = 461 \text{ J kg}^{-1} \text{ K}^{-1}$, $R_d = 287 \text{ J kg}^{-1} \text{ K}^{-1}$, $c_{pd} = 1005 \text{ J kg}^{-1} \text{ K}^{-1}$, $L_v = 2.5 \times 10^6 \text{ J kg}^{-1}$, and $T \in [200, 320] \text{ K}$), the factor $k = \frac{R_v c_{pd} T}{R_d L_v} \in [0.13, 0.21]$. k is a weak function of temperature and is a quasi-constant of order 10^{-1} . In contrast, \tilde{c} scales exponentially with temperature (through q^*) and varies from $\tilde{c}(200 \text{ K}) \sim 10^{-4}$ to $\tilde{c}(320 \text{ K}) \sim 10^1$. The temperature sensitivity of Γ_m is controlled by \tilde{c} . In the dry limit $\tilde{c} \rightarrow 0$, $\Gamma_m \rightarrow \Gamma_d$. In the moist limit $\tilde{c} \rightarrow \infty$, $\Gamma_m \rightarrow k \Gamma_d \sim 0.1 \Gamma_d$, so the moist adiabat cools slowly with height². Because Γ_m is bounded, the magnitude of $\partial\Gamma_m/\partial T$ must peak at some intermediate \tilde{c} .

Where does the magnitude of $\partial\Gamma_m/\partial T$ reach its peak value? To solve this we use the quotient rule on Eq. (13):

$$\frac{\partial\Gamma_m}{\partial T} = \underbrace{\frac{1}{c_{pd} + c_L} \frac{\partial(\alpha_d + \alpha_L)}{\partial T}}_{\text{latent volume sensitivity}} + \underbrace{\left(-\frac{\alpha_d + \alpha_L}{(c_{pd} + c_L)^2} \frac{\partial c_L}{\partial T} \right)}_{\text{latent heat capacity sensitivity}} \quad (18)$$

The latent volume sensitivity varies monotonically with surface temperature (Fig. 3a, c). The non-monotonicity is due to the latent heat capacity sensitivity (Fig. 3b, d) so we further decompose it to identify its origin:

$$-\frac{\alpha_d + \alpha_L}{(c_{pd} + c_L)^2} \frac{\partial c_L}{\partial T} = -\frac{1}{p} \cdot (1 + \tilde{\alpha}) \cdot \frac{R_d}{c_{pd}} \frac{\partial \log c_L}{\partial \log T} \cdot f_d \cdot f_L \quad (19)$$

²This breaks down once water vapor becomes a significant fraction of the atmosphere's mass, i.e. saturation mixing ratio ~ 1 , because the assumption $e^* \ll p$ breaks down.

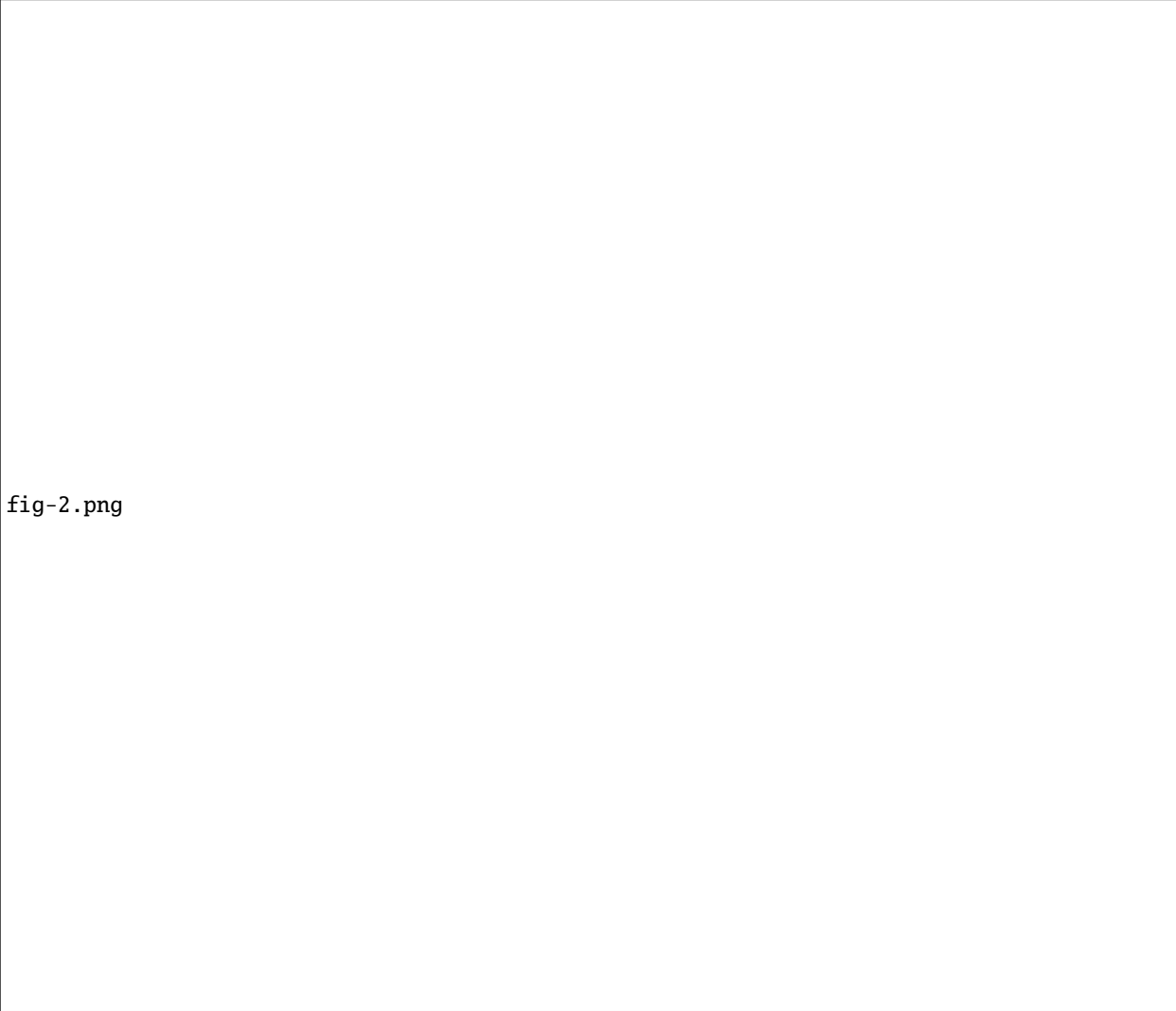


fig-2.png

FIG. 2. (a) The sensitivity of the moist adiabatic lapse rate to surface temperature, $d\Gamma_m/dT_s$, varies non-monotonically with surface temperature. (b) The local minimum of $d\Gamma_m/dT_s$ shifts toward warmer temperatures with surface temperature at higher levels. (c) The sensitivity of the moist adiabatic lapse rate to the local temperature at pressure p , $\partial\Gamma_m/\partial T$, also varies non-monotonically with surface temperature. (d) The integral term in Eq. (7) amplifies the non-monotonicity of $\partial\Gamma_m/\partial T$. (a) is the product of (c) and (d).

where

$$f_d \equiv c_d/(c_{pd} + c_L) \quad (20)$$

$$f_L \equiv c_L/(c_{pd} + c_L) \quad (21)$$

and $f_d + f_L = 1$. f_d and f_L represent the sensible and latent fractions of effective heat capacity, respectively. f_d quantifies the fraction of the moist enthalpy change associated with an increase in sensible enthalpy (i.e. warming) while f_L quantifies the fraction associated with an increase in latent enthalpy (i.e. humidity).

Eq. (19) shows the latent heat capacity sensitivity is a product of four terms that vary monotonically with T . $\tilde{\alpha} = L_v q^*/(\alpha_d p)$ scales exponentially with T through q^* (dashed line in Fig. 4a). The fractional change in la-

tent heat capacity to a fractional change in temperature $\partial \log c_L / \partial \log T = L_v/(R_v T) - 2$ decreases with T (dotted line in Fig. 4a). The product of these two terms is weakly non-monotonic in T with a local minimum located approximately where $\tilde{\alpha} = R_v T/L_v$ (white line in Fig. 4b). At low T , $\tilde{\alpha}$ is small so the product is dominated by the decrease in $\partial \log c_L / \partial \log T$. At high T , $\tilde{\alpha}$ is large so the product is dominated by the exponential increase in $\tilde{\alpha}$. However, the non-monotonicity of these two terms are not the source of the peak magnitude in $\partial\Gamma_m/\partial T$, which requires a local maximum, not a minimum.

The sensible fraction of effective heat capacity f_d logistically decreases with T because c_{pd} is a constant while latent heat capacity c_L increases exponentially with T

fig-3.png

FIG. 3. The moist adiabatic lapse rate sensitivity to local temperature T , $\partial\Gamma_m/\partial T$ (Fig. 2c), is decomposed into contributions from (a) the latent volume sensitivity and (b) the latent heat capacity sensitivity following Eq. (18). (c) The latent volume sensitivity monotonically increases with local temperature T across all pressure levels, e.g. across 500, 400, 300, and 200 hPa. (d) The latent heat capacity sensitivity has a local minimum that shifts toward warmer surface temperature at higher levels, consistent with the behavior of $d\Gamma_m/dT_s$ (Fig. 2b).

through q^* (red line in Fig. 4c). The latent fraction of effective heat capacity f_L logistically increases with T (blue line in Fig. 4c). The product $f_d \cdot f_L$ peaks when $f_d = f_L$, or $c_L = c_{pd}$ (black line in Fig. 4d).

What is the physical intuition behind the peak occurring at $c_L = c_{pd}$? Recall that c_L quantifies the enhancement of effective heat capacity due to condensation heating offsetting adiabatic cooling. Condensation ($\partial_T q^*$ in c_L) requires two ingredients: 1) cooling from expansion and 2) water vapor. f_d and f_L correspond to the fractional availability of the two ingredients. At low T ($c_L < c_{pd}$), condensation is limited by the availability of water vapor (blue line in Fig. 4c). The moist enthalpy response to warming is dominated by an increase in sensible enthalpy (warming).

At high T ($c_L > c_{pd}$), condensation is limited by adiabatic cooling (red line in Fig. 4c), which means the rising parcel retains more water as vapor instead of condensation. The moist enthalpy response to warming is dominated by an increase in latent enthalpy (increase in humidity). The peak in latent heat capacity sensitivity corresponds to where the availability of water vapor and cooling are equally limiting (black line in Fig. 4c). The non-monotonicity in $\partial\Gamma_m/\partial T$ and moist adiabatic warming arises from the competition between the two limiting factors of condensation, which controls the partitioning of the moist enthalpy response to warming into sensible and latent enthalpy.

How well does the condition $c_L = c_{pd}$ capture the actual peak in $\partial\Gamma_m/\partial T$? The theory slightly overpre-

fig-4.png

FIG. 4. The latent heat capacity sensitivity is decomposed into a product of four terms (Eq. 19) that varies monotonically with local temperature T , where local means at pressure p . (a) The latent volume ratio $\tilde{\alpha}$ increases exponentially with T (dashed) while the fractional change in latent heat capacity c_L to a fractional change in T decreases approximately linearly with T (dotted). The product of the two is weakly non-monotonic with T where the product has a local minimum (dash-dot). (b) The local minimum across the pressure-surface temperature space approximately occurs where $\tilde{\alpha} = R_v T / L_v$ (white line). (c) The latent fraction of effective heat capacity f_L increases logistically with T (blue line) while the sensible fraction f_d decreases logistically with T (red line). The product of the two is non-monotonic with T where the product has a local maximum (purple line). (d) The $f_d \cdot f_L$ local maximum across the pressure-surface temperature space occurs where $c_L = c_{pd}$ (black line).

dicts the T_s where the magnitude of $\partial \Gamma_m / \partial T$ peaks (compare solid and dash-dot lines in Fig. 5). This error is due to the weak non-monotonicity in the product $(1 + \tilde{\alpha}) R_d / c_{pd} \partial \log(c_L) / \partial \log(T)$ which decreases with height (Fig. 4b). The error maximizes at the surface where the theory predicts a peak T_s that is 1.6 K warmer than the true peak T_s .

The difference in T_s predicted by the theory and the true peak of Γ_m / dT_s grows with height because the integral term in Eq. (7) amplifies the error in $\partial \Gamma_m / \partial T$ at each level below. This error maximizes at 420 hPa where $c_L = c_{pd}$ predicts a peak T_s that is 2.0 K warmer than the true peak

T_s (compare solid and dashed lines in Fig. 5). This error compounds for T_s of peak moist adiabatic warming ΔT (Eq. 3), leading to a maximum error of 6.6 K at 382 hPa (compare solid and dotted lines in Fig. 5). Thus the condition $c_L = c_{pd}$ is a useful first-order estimate of the T_s where moist adiabatic warming peaks.

3. Implications of the non-monotonicity in moist adiabatic warming on convection

The non-monotonicity of moist adiabatic warming has implications for convective dynamics. For example,

fig-5.png

FIG. 5. Surface temperature T_s corresponding to the criteria $c_L = c_{pd}$ (solid), the minimum of the moist adiabatic lapse rate sensitivity to local temperature $\partial\Gamma_m/\partial T$ (dash dot), the minimum of the moist adiabatic lapse rate sensitivity to surface temperature $d\Gamma_m/dT_s$ (dashed), and the maximum of moist adiabatic warming ΔT (dotted). The theory most accurately captures the T_s corresponding to the minimum of $\partial\Gamma_m/\partial T$. The discrepancy between the theory and the T_s corresponding to the minimum of $d\Gamma_m/dT_s$ and ΔT are larger because the error at pressure p is the accumulation of errors at levels below p (see Eq. 7 and 3).

Roms (2016) showed that parcel buoyancy is a non-monotonic function of surface temperature. Specifically the criterion where B peaks is $\beta = 2c_{pd}$ where

$$\beta = c_{pd} + L_v \frac{\partial q^*}{\partial T} = c_{pd} + c_L \quad (22)$$

Thus the Roms (2016) criterion that maximizes B is equivalent to where moist adiabatic warming peaks, $c_L = c_{pd}$. We show this is true if the entrainment parameter $a = PE\epsilon/g$ is small and derive a more general criterion that maximizes buoyancy³.

Buoyancy B is the normalized virtual temperature (or equivalently, density) difference between the rising parcel $T_{v,p}$ and the environment $T_{v,e}$. Here we neglect the virtual effects of water and use standard temperature:

$$B \approx \frac{g}{T_e} (T_p - T_e) \quad (23)$$

As before, we express temperature profiles in terms of T_s and the integral of their respective lapse rates. We assume the parcel follows a moist adiabatic lapse rate, Γ_m , while the environment is neutrally buoyant with respect to an entraining lapse rate, Γ_e , following the zero-buoyancy

plume model (Singh and O’Gorman 2013):

$$T_p = T_s + \int_{p_s}^p \Gamma_m(p') dp' \quad (24)$$

$$T_e = T_s + \int_{p_s}^p \Gamma_e(p') dp' \quad (25)$$

Substituting Eq. (24) and (25) into the definition of buoyancy Eq. (23) yields

$$B \approx \frac{g}{T_e} \int_{p_s}^p \delta\Gamma dp' \quad (26)$$

where $\delta\Gamma = \Gamma_e - \Gamma_m$. We use the entraining lapse rate Γ_e as in Roms (2016) but expressed in pressure coordinates:

$$\Gamma_e = \Gamma_d \cdot \frac{(1+a)\alpha_d + \alpha_L}{(1+a)c_{pd} + c_L} \quad (27)$$

Substituting Eq. (13) and Eq. (27) into Eq. (26) and simplifying gives

$$B = \frac{g}{T_e} \int_{p_s}^p \Gamma_d \cdot \frac{a(1-k)\tilde{c}}{(1+a+\tilde{c})(1+\tilde{c})} dp' \quad (28)$$

Under the simplifying assumption that entrainment parameter a is constant with T_s , T_e increases monotonically with T_s at all p . Then the origin of the non-monotonicity of B must be in the integrand, $\delta\Gamma$. B depends on T primarily through \tilde{c} , which scales exponentially with T through q^* , whereas Γ_d and k are linear functions of T . In the limit of $\tilde{c} \rightarrow 0$ (cold and dry), $\delta\Gamma$ scales as \tilde{c} , which increases with T . In the limit of $\tilde{c} \rightarrow \infty$ (warm and humid), $\delta\Gamma$ scales as \tilde{c}^{-1} , which decreases with increasing T . This means $\delta\Gamma$ maximizes at some intermediate \tilde{c} .

To solve for the condition that maximizes buoyancy we solve for the \tilde{c} derivative of the integrand $\delta\Gamma$ in Eq. (28) and set it to zero:

$$\frac{d}{d\tilde{c}} \left(\Gamma_d \cdot \frac{a(1-k)\tilde{c}}{(1+a+\tilde{c})(1+\tilde{c})} \right) = 0 \quad (29)$$

If we assume that a , k , and Γ_d do not vary with T , the solution to Eq. (29) is

$$\tilde{c}_{\text{peak}} = \sqrt{1+a} \quad (30)$$

Thus the condition that maximizes buoyancy is $c_L = \sqrt{1+a}c_{pd}$. In the limit of weak entrainment $a \rightarrow 0$, this reduces to $c_L = c_{pd}$. In the presence of entrainment, buoyancy peaks at a higher c_L and so higher T_s all else equal. Entrainment dilutes the air parcel and reduces the latent heat released by the cooling parcel given the same q^* . The factor $\sqrt{1+a}$ describes the shift in the critical point separating the vapor limited and cooling limited regimes toward higher q^* in the presence of entrainment.

³ PE is precipitation efficiency, ϵ is the fractional entrainment rate, and g is gravitational acceleration. See Roms (2016) for the derivation of the entraining plume.

How important is the factor $\sqrt{1+a}$? For an entrainment rate representative of Earth's current climate $a = 0.2$, the difference in T_s of $c_L = c_{pd}$ and $c_L = \sqrt{1+a}c_{pd}$ are < 1.49 K (compare red and solid black line in Fig. 6a). This difference decreases with height and becomes insignificant around the tropopause (0.46 K at $p = 200$ hPa). This is why the criteria $c_L = c_{pd}$ works well for explaining the non-monotonicity of CAPE for present Earth-like climates (Romps 2016). However, for stronger entrainment rates and for understanding the non-monotonicity of buoyancy in the lower troposphere, the factor $\sqrt{1+a}$ becomes more important (e.g., 4.38 K for $a = 0.7$ at the surface; compare red and solid black line in Fig. 6b).

How well do these criteria capture the T_s that maximizes buoyancy across the troposphere? We will first focus on $\delta\Gamma$, i.e. the integrand in Eq. (26). For $a = 0.2$, both criteria capture the T_s of peak $\delta\Gamma$ well (< 1.39 K for $c_L = \sqrt{1+a}c_{pd}$, < 2.87 K for $c_L = c_{pd}$, compare red and solid black line to dashed line in Fig. 6a). The small error arises even for the $c_L = \sqrt{1+a}c_{pd}$ criterion because $\Gamma_d(1-k)$ is weakly non-monotonic with T (Γ_d increases with T and $(1-k)$ decreases with T), which we ignored earlier in order to analytically solve Eq. (29). This error is amplified as we integrate $\delta\Gamma$ to obtain buoyancy Eq. (26) because the error in T_s of peak $\delta\Gamma$ from levels below p accumulates for the T_s of peak B (compare red and solid black line to dotted line in Fig. 6a).

For a higher entrainment parameter $a = 0.7$ the importance of the factor $\sqrt{1+a}$ becomes clear. The error in T_s of peak $\delta\Gamma$ is < 3.39 K for the $c_L = \sqrt{1+a}c_{pd}$ criterion compared to < 5.83 K for the $c_L = c_{pd}$ criterion (compare red and solid black line to dashed line in Fig. 6b). The error in T_s of peak buoyancy is lower for the $c_L = c_{pd}$ criterion (< 3.37 K) compared to the $c_L = \sqrt{1+a}c_{pd}$ criterion (< 4.66 K, compare red and solid black lines to dotted black line in Fig. 6b). This is because $c_L = c_{pd}$ underpredicts T_s for peak B in the lower troposphere, which offsets the growth of the larger error in peak $\delta\Gamma$ (compare solid black and dotted lines in Fig. 6b). The criteria $c_L = c_{pd}$ predicts the T_s of peak buoyancy better than $c_L = c_{pd}\sqrt{1+a}$ in some cases because of a cancelation of errors rather than for the right physical reason. For example the criteria $c_L = c_{pd}$ predicts no shift in T_s that maximizes B to variations in a while the criterion $c_L = \sqrt{1+a}c_{pd}$ qualitatively captures the shift in peak $\delta\Gamma$ and B toward warmer T_s with increasing entrainment (Fig. 6c).

The non-monotonicity of buoyancy with surface temperature extends to the strength of the convective updraft. We model the updraft's specific kinetic energy, $\frac{1}{2}w^2$, using Eq. (1) from Del Genio et al. (2007):

$$\frac{d}{dz} \left(\frac{1}{2} w^2 \right) = a' B(z) - (1 + b') \epsilon(z) w^2 \quad (31)$$

fig-6.png

FIG. 6. Surface temperature T_s corresponding to the criterion $c_L = c_{pd}$ (solid black), the criterion $c_L = c_{pd}\sqrt{1+a}$ (red), the maximum of buoyancy B (dotted), and the minimum of the difference between an entraining lapse rate and moist adiabatic lapse rate $\delta\Gamma = \Gamma_e - \Gamma_m$ (dashed) for the entrainment parameter (a) $a = 0.2$ and (b) $a = 0.7$. (c) The criterion $c_L = c_{pd}\sqrt{1+a}$ captures the a dependence of $\delta\Gamma$ and B extrema evaluated at pressure $p = 500$ hPa. In comparison the criterion $c_L = c_{pd}$ is not sensitive to the entrainment parameter a (vertical black line).

where a' and b' are dimensionless constants. We use $a' = 1/6$ and $b' = 2/3$ following Del Genio et al. (2007). We calculate the fractional entrainment rate $\epsilon(z)$ following Eq. (3) in Romps (2016) with entrainment parameter $a = 0.2$ and precipitation efficiency $PE = 0.35$. Since $w(z)$ is determined by the integral of the net force, which includes buoyancy, we expect updraft velocity to also vary non-monotonically with surface temperature.

Numerically integrating Eq. (31) confirms this expectation. Updraft velocity varies non-monotonically with T_s , updraft velocity decreases with surface temperature at lower levels while it increases with surface temperature at higher levels (Fig. 7a). The surface temperature of peak updraft velocity increases at higher levels, consistent with the non-monotonicity of moist adiabatic warming and buoyancy (Fig. 7b).

Is this result relevant to Earth's atmosphere, where convection is not strictly moist adiabatic and updraft velocity is subject to details and constraints not considered here such as cloud microphysics and radiative cooling? Singh and O'Gorman (2015) shows the 99.99th percentile vertical velocity in CM1 decreases below ≈ 900 hPa and increases above it with surface temperature. While this is qualitatively consistent with the expectations from Eq.(31)(compare our Fig. 7a to their Fig. 2) there are quantitative differences. For example Eq. (31) predicts a decrease in vertical velocity with warming over a deeper layer of the atmosphere (e.g., below $z \approx 11$ km at 300 K) compared to Singh and O'Gorman (2015). To understand the applicability and robustness of the non-monotonicity apparent in Eq. (31), we analyzed updraft velocity in 9 cloud-resolving models simulating radiative convective equilibrium in a 100 km x 100 km domain from the RCEMIP project (Wing et al. 2018). We define updraft velocity as the mean of vertical velocity w exceeding the 99.9th percentile $w > 99.9$ at each height level over the last 25 days of each simulation. The 99.9th percentile corresponds to the fastest 1000 samples of w per level per model. We focus on the strongest convective updrafts because a moist adiabatic profile is most relevant for the convective core of the strongest updrafts (Riehl and Malkus 1958).

There is a large diversity of updraft velocity in the RCEMIP simulations to variations in surface temperature (295, 300, and 305 K, see Fig. 8). Some models exhibit a clear shift toward increasingly top-heavy updraft velocity profiles with warming (e.g., CM1, DAM, UCLA-CRM, UKMO, WRF). In these models, updraft velocity decreases at lower levels, which is qualitatively consistent with Eq. (31) (Fig. 7a). SAM shows a top-heavy shift in updraft velocity without a clear decrease in lower levels. In the remaining models updraft velocity is non-monotonicity with T_s but the T_s of peak updraft velocity does not increase to higher levels as expected from Eq. (31) (Fig. 7b). For example DALES and SCALE predict a non-monotonic response in updraft velocity with T_s at $z \approx 8$ km

but the peak updraft velocity weakens from $T_s = 300$ to 305 K. MesoNH also predicts a decrease in peak updraft velocity from $T_s = 300$ K to 305 K but predicts a non-monotonic response in updraft velocity with T_s at $z \approx 3$ km, much lower than in DALES and SCALE. The diversity of updraft velocity profiles likely arises from differences in model details such as parameterization schemes for cloud microphysics, radiative transfer, and turbulence in addition to emergent behavior such as convective organization. Nonetheless, the presence of non-monotonicity in all but one model suggests that the simple mechanism controlling non-monotonicity in moist adiabatic warming may be playing a role in shaping the variation of updraft velocity profiles across surface temperature in models that explicitly resolve convective storms.

4. Summary and Discussion

Moist adiabatic warming varies non-monotonically with respect to initial surface temperature. The non-monotonicity arises because of a competition between two limiting factors of condensation: availability of water vapor and adiabatic cooling. At low temperature, condensation is limited by the availability of water vapor and moist adiabatic warming scales like Clausius-Clapeyron. At high temperature, condensation is limited by the diminishing net cooling with ascent because high latent heating cancels an increasingly larger fraction of adiabatic cooling. In other words, the moist enthalpy response to warming is dominated by an increase in sensible enthalpy at low temperature and an increase in latent enthalpy at high temperature. The repartitioning of the dominant term in the moist enthalpy response to warming ($c_L = c_{pd}$) corresponds to where moist adiabatic warming peaks. The non-monotonicity of moist adiabatic warming propagates to buoyancy as predicted by the zero-buoyancy plume model because the repartitioning of the moist enthalpy response from sensible to latent enthalpy with increasing temperature occurs in both entraining and moist adiabatic lapse rates. The surface temperature where the buoyancy peaks follows $c_L = c_{pd}\sqrt{1+a}$, where a is the entrainment parameter as defined in Romps (2016). The non-monotonicity of buoyancy also propagates to updraft velocity. Cloud-resolving models simulating radiative-convective equilibrium exhibit diverse but qualitatively consistent responses of strong convective updrafts to surface temperature changes as predicted by the zero-buoyancy plume model.

Seeley and Romps (2016) first noted the importance of the $c_L = c_{pd}$ criteria to explain why buoyancy profiles are top heavy. Buoyancy maximizes where the saturation moist static energy difference between the environment and parcel (δh^*) are expressed as a temperature difference (sensible enthalpy difference, $c_{pd}\delta T$) rather than a humidity difference (latent enthalpy difference, $L_v\delta q^*$). The ratio $\tilde{c} = c_L/c_{pd} = L_v\delta q^*/(c_{pd}\delta T)$ quantifies the transition

fig-7.png

FIG. 7. (a) Vertical profiles of updraft velocity, calculated by numerically integrating Eq. (31) in height using buoyancy B from Eq. (23). Updraft velocity decreases with surface temperature at lower levels while it increases with surface temperature at higher levels. (b) Updraft velocity varies non-monotonically with surface temperature at all levels, e.g. at 5, 10, 15, and 20 km. Updraft velocity peaks at warmer surface temperatures at higher levels consistent with the behavior of buoyancy (Fig. 6a) and moist adiabatic warming (Fig. 5).

where δh^* is expressed largely in terms of $L_v \delta q^*$ (lower troposphere, where $\tilde{c} > 1$) and in terms of $c_{pd} \delta T$ (upper troposphere, where $\tilde{c} < 1$). Seeley and Roms (2015) showed that buoyancy at a fixed level varies non-monotonically with surface temperature (see their Fig. 2a) and Roms (2016) explained the non-monotonicity of buoyancy at the tropopause to explain the non-monotonicity of CAPE with surface temperature. Following the same reasoning as in Seeley and Roms (2016), Roms (2016) shows that tropopause buoyancy and CAPE peak where $c_L = c_{pd}$. We show that a more general criterion for the T_s of peak buoyancy is $c_L = c_{pd} \sqrt{1+a}$, which reduces to $c_L = c_{pd}$ in the limit of weak entrainment. The factor $\sqrt{1+a}$ is insignificant in Earth's current climate (e.g. for $a = 0.2$, $\sqrt{1+a} = 1.09$) so Roms (2016)'s criterion works well for understanding the non-monotonicity of CAPE on Earth-like atmospheres. However, the factor $\sqrt{1+a}$ is important for understanding the non-monotonicity of buoyancy at lower levels and CAPE in a world with stronger entrainment rates than on present-day Earth.

Curiously, the surface temperature of peak CAPE (≈ 335 K, Roms 2016) is similar to the surface temperature that marks the transition to a moist greenhouse regime (≈ 335 K, Komabayasi 1967; Ingersoll 1969; Kasting 1988). Is this similarity due to a shared physical mechanism or a coincidence? The criteria for peak CAPE is $L_v (\partial_T q^*)|_{\text{tropopause}} = c_{pd}$, i.e. the surface temperature where the *temperature sensitivity* of latent and sen-

sible enthalpy at the *tropopause* are equal. On the other hand the criteria for the transition to a moist greenhouse is $L_v q_s^* = c_{pd} T_s$, i.e. the surface temperature where the *magnitude* of latent and sensible enthalpy at the *surface* are equal (Wordsworth and Pierrehumbert 2013). The ratio of the temperature sensitivity of latent and sensible enthalpy at the tropopause scales differently from the ratio of the magnitude of latent and sensible enthalpy at the surface (Fig. D1, see Appendix D for more detail). While these threshold coincide around 335 K in Earth-like climates, their underlying scalings differ, suggesting that they may diverge in other planetary climates.

The non-monotonicity of moist adiabatic warming may have additional implications for climate, such as the organization of convection and the large-scale circulation response to warming. For example, Shaw and Miyawaki (2025) explain the mechanism behind the 2% K^{-1} scaling of the mean and extreme upper-level wind response to warming by assuming a moist adiabatic atmosphere. The non-monotonicity of moist adiabatic warming would drive a non-monotonic change in the meridional and zonal temperature gradients at fixed height or pressure levels. This could serve as a thermodynamically driven hypothesis for the potential of non-monotonicities to emerge in dynamical responses to warming such as in the response of jet stream wind, extratropical cyclones, and mean overturning circulations.

fig-8.png

FIG. 8. Updraft velocity from 9 cloud-resolving models (CM1, DALES, DAM, MesoNH, SAM-CRM, SCALE, UCLA-CRM, UKMO-CASIM, and WRF) that participated in RCEMIP (Wing et al. 2018). The simulations are on a $100 \text{ km} \times 100 \text{ km}$ periodic domain for uniform sea surface temperatures set to 295 (blue), 300 (black), and 305 K (red). Updraft velocity at each level is the mean of vertical velocities w that exceed the 99.9th percentile ($w_{>99.9}$).

Acknowledgments. I thank the Union College Faculty Research Fund and the NSF National Center for Atmospheric Research Advanced Studies Program for supporting this work. I thank Andrew Williams, Jiawei Bao, Jonah Bloch-Johnson, Martin Singh, Stephen Po-Chedley, Nadir Jeevanjee, and two anonymous reviewers for helpful discussions and feedback on the manuscript.

Data availability statement. All scripts used for analysis and plots in this paper are available at <https://github.com/omiyawaki/miyawaki-2025-nonmonotonic-moist-adiabat>. They will also be archived on Zenodo upon publication.

APPENDIX A

Calculating Moist Adiabatic Profiles

We calculate moist adiabatic profiles numerically by assuming the conservation of saturation moist static energy h^* :

$$h^* = c_{pd}T + gz + L_v q^* \quad (\text{A1})$$

where T is temperature, z is height, q^* is the saturation specific humidity, g is the acceleration due to gravity on Earth, c_{pd} is the specific heat of dry air at constant pressure, and L_v is the latent heat of vaporization. We use the Bolton (1980) formula for saturation vapor pressure e^* (Eq. C1). The values we use for all thermodynamic constants are in Table A1.

We first calculate surface saturation moist static energy h_s^* for a given surface temperature T_s and surface pressure p_s . We calculate h^* at higher levels in -50 hPa pressure increments. We assume hydrostatic balance to calculate the height z_{i+1} at the next pressure level p_{i+1} . We solve for T_{i+1} that satisfies the condition $h_{i+1}^* = h_s^*$ using Brent's root-finding method (`scipy.optimize.root_scalar` with `method=brentq`).

We also show moist adiabatic warming in height coordinates to demonstrate that the non-monotonicity is not an artifact of the choice of the vertical coordinate (Fig. A1). We follow the same procedure as above except we step to higher levels in 100 m height increments.

APPENDIX B

Sensitivity of Non-monotonicity to Fusion

We assess how latent heat of fusion influences the non-monotonicity of moist adiabatic warming. Following Flannaghan et al. (2014), we represent freezing following the

IFS Cycle 40 documentation (ECMWF 2022). The fraction of liquid water α varies with T as follows

$$\alpha(T) = \begin{cases} 0, & T \leq T_{\text{ice}} \\ \left(\frac{T - T_{\text{ice}}}{T_0 - T_{\text{ice}}} \right)^2, & T_{\text{ice}} < T < T_0 \\ 1, & T \geq T_0 \end{cases} \quad (\text{B1})$$

where $T_{\text{ice}} = 253.15$ K and $T_0 = 273.15$ K. All condensate is ice below 253.15 K, all condensate is liquid above 273.15 K, and the transition between the two limits is quadratic.

The saturation vapor pressure e^* is the weighted average over liquid (e_ℓ^*) and ice (e_i^*):

$$e^* = \alpha e_\ell^* + (1 - \alpha) e_i^* \quad (\text{B2})$$

The saturation vapor pressure over liquid and ice is

$$e_{\ell,i}^*(T) = a_1 \exp \left(a_3 \frac{T - T_0}{T - a_4} \right) \quad (\text{B3})$$

where over liquid $a_1 = 611.21$ Pa, $a_3 = 17.502$, $a_4 = 32.19$ K (Buck 1981) and over ice $a_1 = 611.21$ Pa, $a_3 = 22.587$, $a_4 = -0.7$ K (Alduchov and Eskridge 1996).

The effective latent heat of vaporization $L_e^*(T)$ includes both condensation and fusion:

$$L_e^*(T) = L_v + (1 - \alpha) L_f \quad (\text{B4})$$

where $L_f = 0.334 \times 10^6$ J kg⁻¹ is the latent heat of fusion.

Moist adiabats including fusion are obtained by solving for T that conserves the saturation moist static energy with the effective latent heat L_e :

$$h_{\text{fusion}}^* = c_{pd}T + gz + L_e q^* \quad (\text{B5})$$

The non-monotonicity of moist adiabatic warming emerges with or without fusion (compare Fig. 1b and B1a). Fusion introduces a secondary local maximum of warming due to the additional energy release from fusion (Fig. B1b). When the secondary peak is to the right of the primary peak the T_s of peak warming shifts to colder T_s (points below the 1:1 line in Fig. B1c). As the secondary peak overlaps with the primary peak, the T_s of peak warming shifts to warmer T_s with fusion (points above the 1:1 line in Fig. B1c). This effect is largest (6.01 K) at 727 hPa. Since fusion represents a secondary effect and complicates the analysis, we neglect it in the main analysis.

APPENDIX C

Sensitivity of Non-monotonicity to Saturation Vapor Pressure Formulas

fig-a1.png

FIG. A1. (a) Vertical profiles of moist adiabatic warming to a 4 K surface warming for $T_s = 280, 290, 300, 310,$ and 320 K. Warming decreases with initial surface temperature at lower levels while it increases with initial surface temperature at higher levels. (b) Moist adiabatic warming varies non-monotonically with initial surface temperature at all levels, e.g. at 5 km, 10 km, 15 km, and 20 km. Moist adiabatic warming peaks at warmer initial surface temperatures at higher levels.

TABLE A1. Thermodynamic constants used in this study.

Symbol	Description	Value	Units
g	Acceleration due to gravity	9.81	m s^{-2}
c_p	Specific heat of dry air	1005.7	$\text{J kg}^{-1} \text{K}^{-1}$
R_d	Gas constant of dry air	287.05	$\text{J kg}^{-1} \text{K}^{-1}$
R_v	Gas constant of water vapor	461.5	$\text{J kg}^{-1} \text{K}^{-1}$
ϵ	Ratio of gas constants (R_d/R_v)	0.622	dimensionless
p_s	Surface pressure	1000	hPa
L_v	Latent heat of vaporization	2.501×10^6	J kg^{-1}

The moist adiabatic lapse rate depends on the choice of the empirical formula for saturation vapor pressure e^* . To assess the sensitivity of the non-monotonicity in moist adiabatic warming to different empirical fits of $e^*(T)$, we test how the T_s of peak warming varies across three formulas: Bolton (1980), Goff-Gratch (as described in List 1949), and Murphy and Koop (2005).

The Bolton (1980) formula is:

$$e^* = 6.112 \exp\left(\frac{17.67(T - 273.15)}{T - 29.65}\right) \quad [\text{hPa}] \quad (\text{C1})$$

The Goff-Gratch formula is:

$$\begin{aligned} \log_{10} e^* = & -7.90298 \left(\frac{373.16}{T} - 1 \right) \\ & + 5.02808 \log_{10} \left(\frac{373.16}{T} \right) \\ & - 1.3816 \times 10^{-7} \left(10^{11.344(1-T/373.16)} - 1 \right) \\ & + 8.1328 \times 10^{-3} \left(10^{-3.49149(373.16/T-1)} - 1 \right) \\ & + \log_{10}(1013.246) \quad [\text{hPa}] \quad (\text{C2}) \end{aligned}$$

fig-b1.png

FIG. B1. Moist adiabatic warming ΔT for 4 K surface warming including latent heat of fusion. (a) Warming decreases at lower levels with initial surface temperatures (T_s) while it increases at upper levels with T_s for 280, 290, 300, 310, and 320 K. (b) Warming peaks at warmer T_s at higher pressure levels, e.g. at 500, 400, 300, and 200 hPa. (c) T_s corresponding to peak warming with and without fusion are comparable at upper levels (> 500 hPa) but can deviate up to 6.01 K at lower levels (< 500 hPa).

The Murphy and Koop (2005) formula is:

$$\ln e^* = 54.842763 - \frac{6763.22}{T} - 4.210 \ln T + 0.000367T + \tanh(0.0415(T - 218.8)) \left(53.878 - \frac{1331.22}{T} - 9.44523 \ln T + 0.014025T \right) \quad [\text{Pa}] \quad (\text{C3})$$

where T is in Kelvin for all 3 formulas.

Bolton (1980) is sufficiently accurate for the purposes of evaluating the T_s that leads to maxima in moist adiabatic warming (Fig. C1). The differences in peak T_s across the three saturation vapor pressure formulas are small. The largest difference in T_s of peak warming is 0.11 K at 903 hPa between Bolton and Goff-Gratch and 0.16 K at 901 hPa between Bolton and Murphy-Koop. We choose to use Bolton (1980) in the main analysis due to its simplicity.

fig-c1.png

FIG. C1. (a) T_s corresponding to peak warming using Bolton (1980) and Goff-Gratch saturation vapor pressure formula are similar (difference is < 0.11 K). (b) Same as (a) but comparing Bolton (1980) and Murphy and Koop (2005), which also predicts similar T_s of peak warming (difference is < 0.16 K).

APPENDIX D

Criteria for Moist Greenhouse and Peak CAPE

The moist greenhouse transition occurs when high water vapor concentration in the stratosphere lead to increased photolysis of water vapor and hydrogen escape. The criterion for the onset of this regime is when the magnitude

of the latent to sensible enthalpy at the surface are equal (Wordsworth and Pierrehumbert 2013):

$$\frac{L_v q_s^*}{c_{pd} T_s} = 1 \quad (\text{D1})$$

In contrast, peak CAPE corresponds to the surface temperature where the temperature sensitivity ratio of latent and sensible enthalpy at the tropopause are equal (which works well for $a \ll 1$, Roms 2016):

$$\frac{c_{L,t}}{c_{pd}} = \frac{L_v}{c_{pd}} \left. \frac{\partial q^*}{\partial T} \right|_t = 1 \quad (\text{D2})$$

where the subscript t is the tropopause. Combining Eq. (D2) and Eq. (11) in this paper together with Eq. (15) in Roms (2016):

$$\left. \frac{dq^*}{dT} \right|_t \approx \frac{\epsilon}{p_s} \left(\frac{de_t^*}{dT} \exp(A(T_s - T_t) + B) - A e^* \exp(A(T_s - T_t) + B) \right) \quad (\text{D3})$$

where $A = \frac{c_{pd}}{R_d T_0}$, $B = \frac{L_v q_s^*}{(1+a) R_d T_0}$, and $T_0 = \frac{T_s + T_t}{2}$. Following Roms (2016) we set $a = 0$ and $T_t = 200$ K when calculating Eq. (D3).

The T_s of the transition to the moist greenhouse regime (332.9 K, where the blue line equals 1 in Fig. D1) and peak CAPE (337.8 K, where the orange line equals 1 in Fig. D1) are similar, both occurring ≈ 335 K. However, the T_s that satisfy each criteria emerge from nondimensional numbers that scale differently with T_s . The moist greenhouse criterion proposed by Wordsworth and Pierrehumbert (2013) is only a function of surface moist enthalpy partitioning. The peak CAPE criterion is not only a function of surface moist enthalpy but also the tropopause temperature T_t , which is influenced by both moist thermodynamics and radiative transfer (e.g., Held 1982; Hu and Vallis 2019). Thus there is no *a priori* expectation that the surface temperatures corresponding to these two transitions must coincide across a broad range of planetary climates.

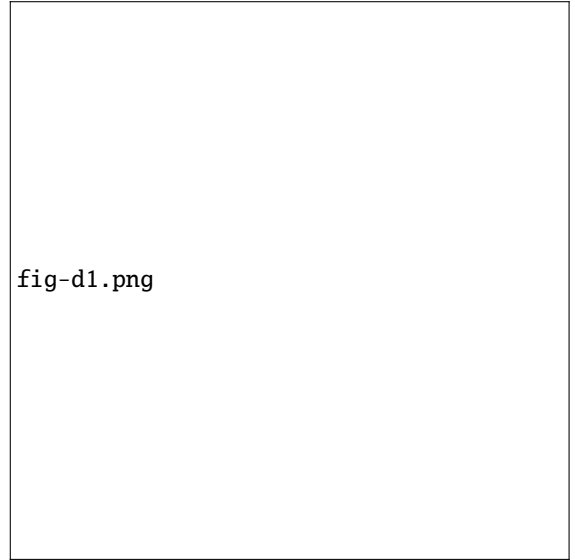


fig-d1.png

FIG. D1. Although the T_s of the transition to a moist greenhouse regime and peak CAPE are both ≈ 335 K, they arise from different criteria. The transition to a moist greenhouse regime corresponds to where the magnitude of latent and sensible enthalpy are equal (blue line equals 1). Peak CAPE corresponds to where the temperature sensitivity of latent and sensible enthalpy are equal (orange line equals 1).

References

- Alduchov, O. A., and R. Eskridge, 1996: Improved magnus form approximation of saturation vapor pressure. *Journal of Applied Meteorology*, **35** (4), 601–609.
- Arakawa, A., and W. H. Schubert, 1974: Interaction of a cumulus cloud ensemble with the large-scale environment, part I. *Journal of the Atmospheric Sciences*, **31** (3), 674–701.
- Bao, J., V. Dixit, and S. C. Sherwood, 2022: Zonal temperature gradients in the tropical free troposphere. *Journal of climate*.
- Bolton, D., 1980: The computation of equivalent potential temperature. *Mon. Weather Rev.*, **108** (7), 1046–1053.
- Buck, A. L., 1981: New equations for computing vapor pressure and enhancement factor. *Journal of Applied Meteorology and Climatology*, **20** (12), 1527–1532.
- Byrne, M. P., and P. A. O’Gorman, 2013: Land–ocean warming contrast over a wide range of climates: Convective quasi-equilibrium theory and idealized simulations. *Journal of climate*, **26** (12), 4000–4016.
- Del Genio, A. D., M.-S. Yao, and J. Jonas, 2007: Will moist convection be stronger in a warmer climate?: CONVECTION STRENGTH IN a WARMER CLIMATE. *Geophys. Res. Lett.*, **34** (16).
- ECMWF, 2022: IFS documentation. Accessed: 2025-10-28, <https://www.ecmwf.int/en/publications/ifs-documentation>.
- Emanuel, K. A., 1994: *Atmospheric Convection*. Oxford University Press.
- Flannaghan, T. J., S. Fueglistaler, I. M. Held, S. Po-Chedley, B. Wyman, and M. Zhao, 2014: Tropical temperature trends in atmospheric general circulation model simulations and the impact of uncertainties in observed SSTs. *Journal of Geophysical Research, D: Atmospheres*, **119** (23), 13,327–13,337.
- Hansen, J., A. Lacis, D. Rind, G. Russell, P. Stone, I. Fung, R. Ruedy, and J. Lerner, 1984: Climate sensitivity: Analysis of feedback mechanisms. *Climate Processes and Climate Sensitivity*, American Geophysical Union (AGU), 130–163.
- Hartmann, D. L., and K. Larson, 2002: An important constraint on tropical cloud - climate feedback. *Geophysical research letters*, **29** (20), 12–1–12–4.
- Held, I. M., 1982: On the height of the tropopause and the static stability of the troposphere. *Journal of the Atmospheric Sciences*, **39** (2), 412–417.
- Held, I. M., 1993: Large-scale dynamics and global warming. *Bull. Am. Meteorol. Soc.*, **74** (2), 228–242.
- Held, I. M., and K. M. Shell, 2012: Using relative humidity as a state variable in climate feedback analysis. *Journal of climate*, **25** (8), 2578–2582.
- Held, I. M., and B. J. Soden, 2000: Water vapor feedback and global warming. *Annual review of energy and the environment*, **25** (1), 441–475.
- Hu, S., and G. K. Vallis, 2019: Meridional structure and future changes of tropopause height and temperature. *Quarterly Journal of the Royal Meteorological Society*, **145** (723), 2698–2717.
- Ingersoll, A. P., 1969: The runaway greenhouse: A history of water on venus. *Journal of the atmospheric sciences*, **26** (6), 1191–1198.
- Kasting, J., 1988: Runaway and moist greenhouse atmospheres and the evolution of earth and venus. *Icarus*, **74**, 472–494.
- Keil, P., H. Schmidt, B. Stevens, and J. Bao, 2021: Variations of tropical lapse rates in climate models and their implications for upper tropospheric warming. *Journal of climate*, **34** (24), 1–50.
- Komabayasi, M., 1967: Discrete equilibrium temperatures of a hypothetical planet with the atmosphere and the hydrosphere of one component-two phase system under constant solar radiation. *Journal of the Meteorological Society of Japan*, **45** (1), 137–139.
- Levine, X. J., and W. R. Boos, 2016: A mechanism for the response of the zonally asymmetric subtropical hydrologic cycle to global warming. *J. Clim.*, **29** (21), 7851–7867.
- List, R. J., 1949: Smithsonian meteorological tables. *Smithsonian miscellaneous collections*, **114**, 1–521.
- Miyawaki, O., Z. Tan, T. A. Shaw, and M. F. Jansen, 2020: Quantifying key mechanisms that contribute to the deviation of the tropical warming profile from a moist adiabat. *Geophys. Res. Lett.*, **47** (20), e2020GL089136.
- Murphy, D. M., and T. Koop, 2005: Review of the vapour pressures of ice and supercooled water for atmospheric applications. *Quarterly journal of the Royal Meteorological Society. Royal Meteorological Society (Great Britain)*, **131** (608), 1539–1565.
- Neelin, J. D., and I. M. Held, 1987: Modeling tropical convergence based on the moist static energy budget. *Mon. Weather Rev.*, **115** (1), 3–12.
- O’Gorman, P. A., 2015: Precipitation extremes under climate change. *Current climate change reports*, **1** (2), 49–59.
- Riehl, H., and J. S. Malkus, 1958: On the heat balance of the equatorial trough zone. *Geophysica*, **6** (3–4).
- Romps, D. M., 2016: Clausius–Clapeyron scaling of CAPE from analytical solutions to RCE. *J. Atmos. Sci.*, **73** (9), 3719–3737.
- Santer, B. D., and Coauthors, 2005: Amplification of surface temperature trends and variability in the tropical atmosphere. *Science*, **309** (5740), 1551–1556.
- Seeley, J. T., N. Jeevanjee, and D. M. Romps, 2019: FAT or FiTT: Are anvil clouds or the tropopause temperature invariant? *Geophysical research letters*, **46** (3), 1842–1850.
- Seeley, J. T., and D. M. Romps, 2015: Why does tropical convective available potential energy (CAPE) increase with warming? *Geophysical research letters*, **42** (23), 10,429–10,437.
- Seeley, J. T., and D. M. Romps, 2016: Tropical cloud buoyancy is the same in a world with or without ice. *Geophysical research letters*, **43** (7), 3572–3579.
- Shaw, T. A., and O. Miyawaki, 2025: Moist adiabatic scaling explains mean and fast upper-level jet stream wind response to climate change. *Geophysical research letters*, **52** (20), e2025GL118315.
- Shaw, T. A., and A. Voigt, 2016: What can moist thermodynamics tell us about circulation shifts in response to uniform warming? *Geophysical research letters*, **43** (9), 4566–4575.
- Singh, M. S., and P. A. O’Gorman, 2013: Influence of entrainment on the thermal stratification in simulations of radiative-convective equilibrium. *Geophysical research letters*, **40** (16), 4398–4403.

- Singh, M. S., and P. A. O’Gorman, 2015: Increases in moist-convective updraught velocities with warming in radiative-convective equilibrium. *Quarterly Journal of the Royal Meteorological Society*, **141** (692), 2828–2838.
- Vallis, G. K., P. Zurita-Gotor, C. Cairns, and J. Kidston, 2015: Response of the large-scale structure of the atmosphere to global warming. *Quart. J. Roy. Meteor. Soc.*, **141** (690), 1479–1501.
- Wing, A. A., K. A. Reed, M. Satoh, B. Stevens, S. Bony, and T. Ohno, 2018: Radiative–convective equilibrium model intercomparison project. *Geoscientific Model Development*, **11** (2), 793–813.
- Wordsworth, R. D., and R. T. Pierrehumbert, 2013: WATER LOSS FROM TERRESTRIAL PLANETS WITH CO₂-RICH ATMOSPHERES. *The Astrophysical Journal*, **778** (2), 154.